ISSN 0010-5082, Combustion, Explosion, and Shock Waves, 2023, Vol. 59, No. 5, pp. 582–590. © Pleiades Publishing, Ltd., 2023.
Russian Text © A.P. Ershov.

On Electromagnetic Measurements of Particle Velocity

A. P. Ershov[a,*]

UDC 662.215.1

Published in *Fizika Goreniya i Vzryva*, Vol. 59, No. 5, pp. 53–62, September–October, 2023.
Original article submitted September 28, 2022; revision submitted November 02, 2022;
accepted for publication December 14, 2022.

Abstract: One of the shortcomings of the classical electromagnetic method of Zavoisky is sensitivity to the non-one-dimensionality of the flow behind the wave front. In this paper, it is proposed to use a four-pin gauge to correct measurements. Two signals are recorded from Π-shaped gauges, one of which is located in a plane tangent to the front, and the other in a plane parallel to the direction of wave propagation. Next, the two signals are combined into a true velocity signal that is insensitive to the curvature of the front. The second difficulty that arises in electromagnetic measurements is the rather large size of the gauges. Typically, the length of the working arm L is about 1 cm. An analysis of the potential distribution in the gauge shows that the proposed combined gauge is equivalent to two sensors of zero width, and the effective length L is the distance between the midlines of the leads. It is shown that the value of L can be reduced to 1.5–2 mm with a lead width of about 0.5 mm. This makes it possible to perform local measurements at spots of millimeter size and use small-size charges. These improvements bring electromagnetic measurements closer to the level of modern optical techniques while using much cheaper equipment.

Keywords: detonation, explosion, experiment, electromagnetic method.

DOI: 10.1134/S0010508223050076

INTRODUCTION

The electromagnetic method proposed by Zavoisky in 1947 [1] began to be widely used for particle velocity measurements in shock and detonation waves since the 1960s [2, 3]. The signal of the velocity u is measured by a Π-shaped gauge made of thin foil entrained by the motion of the medium in a magnetic field. The voltage V across the leads of the gauge is:

$$V = BLu \tag{1}$$

(B is the magnetic induction and L is the length of the working arm of the gauge).

Over the past decades, numerous improvements of the method have been developed. Various geometries of gauges have been tested (see, e.g., [4]). The use of increasingly thinner foils has made it possible to improve the time resolution to ≈10 ns [5], and the use of a set of many gauges in one experiment has given an opportunity to trace the evolution of propagating waves [6]. An advantage of the electromagnetic method is that it is based on the basic physical principle—Faraday's law. However, significant shortcomings of this approach have been found in practice.

First, in experiments, rather wide sensors with working arm length $L \simeq 1$ cm are used as a rule. This choice of the size is dictated by both the ease of fabrication and the desire to observe the gauge geometry in which the width of the gauge leads is much smaller than L. Meanwhile, the leads cannot be arbitrarily narrow for durability reasons. As a result, the spatial resolution suffers: the measured velocity is averaged over the scale L. Moreover, this leads to stringent requirements for the dimensions of the test object. For example, for detonation flow, the diameter of the explosive charge should far exceed L.

Second, in studies of an explosion, the flow is typically non-one-dimensional. Most studies are carried out with cylindrical charges in which the steady wave front

[a]Lavrent'ev Institute of Hydrodynamics, Siberian Branch, Russian Academy of Sciences, Novosibirsk, 630090 Russia; *ers@hydro.nsc.ru.

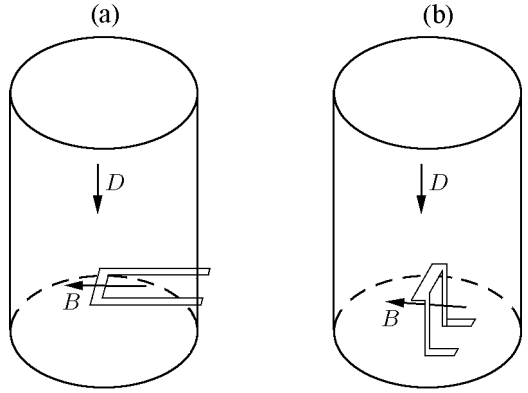

Fig. 1. Flat velocity gauge (a) and a bent gauge with leads parallel to the flow (b) placed in a cylindrical charge.

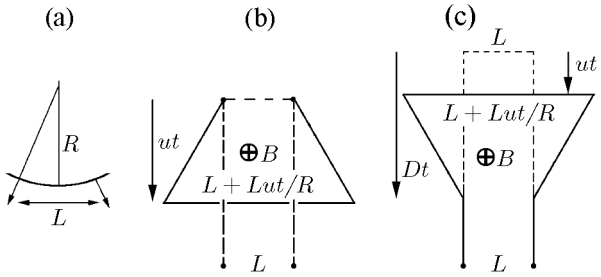

Fig. 2. Displacement directions in a spherical wave (a) and the projections of the contours of the flat gauge (b) and the bent gauge (c) onto the plane perpendicular to the magnetic field (deformations are shown for constant velocities D and u).

has some curvature. The side expansion of the material sets in motion not only the active element, but also the gauge leads, which generates a spurious signal that distorts the measurement results. Rather intricate measures have been taken to reduce this error [7].

The above-mentioned shortcomings are not typical for modern laser optical methods: VISAR, ORVIS, PDV, etc., which allow measurements in spots of submillimeter size and are insensitive to the wave curvature. Therefore, in recent years, electromagnetic diagnostics has been gradually replaced by optical approaches. However, laser techniques are much more expensive, so that a certain niche for the electromagnetic method is still preserved.

In this paper, it is proposed to modify the electromagnetic diagnostics to eliminate the above disadvantages. This makes it possible to bring electromagnetic measurements closer to the level of modern optical techniques while using much cheaper equipment.

INFLUENCE OF FRONT CURVATURE

In this section, we consider two velocity gauges shown in Fig. 1. The flat gauge (Fig. 1a) is easier to fabricate: there is only one contact surface on which it is placed. For the bent gauge (Fig. 1b), whose leads are oriented along the direction of wave propagation, an additional gluing surface is required. Sometimes, a flat sensor is called a Lorenz gauge, and a bent sensor or similar configurations are referred to as Faraday gauges [8], although this terminology is hardly appropriate. In both cases, a signal can be regarded either as a result of the Lorentz force in the moving conductor or as a consequence of magnetic flux changes through the moving contour.

During the detonation of a cylindrical charge, the wave front becomes convex in the direction of propagation due to side expansion. As a first approximation, we assume that the radius of curvature of the front R is constant during the measurement. Curvature leads to lateral displacements (Fig. 2a). We consider the influence of front curvature on the gauge signal, neglecting the width of the gauge leads. The influence of finite width is discussed in Appendix. We also assume that the displacements in the lateral direction are small compared to longitudinal displacements.

Figures 2b and 2c show the deformations of the gauge contours during their involvement in the movement of the medium. In both cases, the crossbar of the gauge is lengthened due to curvature.

We first consider the flat gauge. Let the movement of its crossbar starts at the moment $t = 0$. Due to the curvature, the leads start moving later. We find the gauge signal at $t \geq 0$. The distance between the elements of the leads that were set in motion at time τ $(0 < \tau < t)$ is

$$l(t,\tau) = L\Big(1 + \frac{1}{R}\int\limits_0^{t-\tau} u(\eta)\,d\eta\Big). \qquad (2)$$

The flow velocity u behind the wave front depends on time; η denotes the time counted from the beginning of the motion of this element. The displacement in the direction of wave propagation is given by

$$z(t,\tau) = \int\limits_0^{t-\tau} u(\eta)\,d\eta.$$

It can be seen from these formulas that for any dependence of the velocity u on time, the deformed part of the contour has the shape of a trapezoid. The contour area for the flat gauge is

$$S_= = S_0 - \Big(L + \frac{L}{2R}\int\limits_0^t u(\eta)\,d\eta\Big)\int\limits_0^t u(\eta)\,d\eta,$$

where S_0 is the initial area of the contour. The output voltage is

$$V_= = -B\,\frac{dS_=}{dt} = BLu(t)\Big(1 + \frac{1}{R}\int\limits_0^t u(\eta)\,d\eta\Big). \quad (3)$$

For the bent gauge, the calculations are somewhat more complicated. The width of the contour element that starts moving at the moment τ is still given by formula (2). The corresponding vertical coordinate is

$$z(t,\tau) = D\tau + \int\limits_0^{t-\tau} u(\eta)\,d\eta, \quad \frac{\partial z}{\partial \tau} = Du(t-\tau),$$

where D is the wave front velocity. The minimum value of $z(t,\tau)$ is $z(t,0) = \int\limits_0^t u(\eta)\,d\eta$ and the maximum value is $z(t,\tau) = Dt$. Now the contour shape is generally not a trapezoid. The change in the area of the contour is

$$S_\parallel = \int\limits_{z(t,0)}^{z(t,t)} l\,dz - LDt = \int\limits_0^t l(t,\tau)\,\frac{\partial z}{\partial \tau}\,d\tau - LDt$$

or

$$S_\parallel = L\Big(-\int\limits_0^t u(t-\tau)\Big(1 + \frac{1}{R}\int\limits_0^{t-\tau} u(\eta)\,d\eta\Big)\,d\tau + \frac{D}{R}\int\limits_0^t d\tau \int\limits_0^{t-\tau} u(\eta)\,d\eta\Big).$$

After the partial replacement $t - \tau = \eta$ and the change in the notation of the internal variable of integration, we get

$$S_\parallel = L\Big(-\int\limits_0^t u(\eta)\,d\eta\Big(1 + \frac{1}{R}\int\limits_0^\eta u(\xi)\,d\xi\Big) + \frac{D}{R}\int\limits_0^t d\tau \int\limits_0^{t-\tau} u(\xi)\,d\xi\Big).$$

The output signal of the gauge is

$$V_\parallel = -B\,\frac{dS_\parallel}{dt} = BLu(t)\Big(1 + \frac{1}{R}\int\limits_0^t u(\xi)\,d\xi\Big) - \frac{BLD}{R}\int\limits_0^t u(t-\tau)\,d\tau,$$

which can be rewritten as

$$V_\parallel = -B\,\frac{dS_\parallel}{dt} = BLu(t)\Big(1 + \frac{1}{R}\int\limits_0^t u(\eta)\,d\eta\Big) - \frac{BLD}{R}\int\limits_0^t u(\eta)\,d\eta. \quad (4)$$

The difference with (3) is in the last (negative) term. Thus, at the initial time $t = 0$, the readings of the flat and bent gauges coincide, but as t increases, they become different. Omitting the constant BL, we introduce two directly measured velocities:

$$u_= = u(t)\Big(1 + \frac{1}{R}\int\limits_0^t u(\eta)\,d\eta\Big), \qquad u_\parallel = u_= - \frac{D}{R}\int\limits_0^t u(\eta)\,d\eta. \quad (5)$$

It can be seen that $u_=$ is greater and $u_\parallel$ is lower than the true velocity $u(t)$. Naturally, the idea arises of retrieving the true velocity from two data sets $u_=(t)$ and $u_\parallel(t)$.

Above, the front velocity D was assumed to be constant, which corresponds to measurements in a steady detonation wave. In practice, the gauge is often placed at the end of the charge, and then a then gradually fading shock wave propagates into the window material. But in this case, too, for the problem under consideration, the change in D can usually be neglected since the wave velocity is a more conservative quantity compared to the particle velocity $u(t)$, and the introduced correction, as will be seen, is small. In the case $D = \text{const}$, we have

$$u_= - u_\parallel = \frac{D}{R}\int\limits_0^t u(\eta)\,d\eta.$$

The last expression allows us to explicitly take into account the error in the measurement of $u_=$:

$$u(t) = \frac{u_=}{1 + \dfrac{1}{R}\displaystyle\int\limits_0^t u(\eta)\,d\eta} = \frac{u_=}{1 + \dfrac{u_= - u_\parallel}{D}}. \quad (6)$$

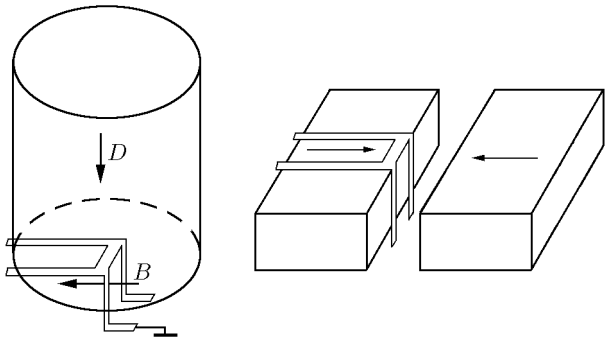

Fig. 3. Measurement geometry using the combined probe and its location before gluing.

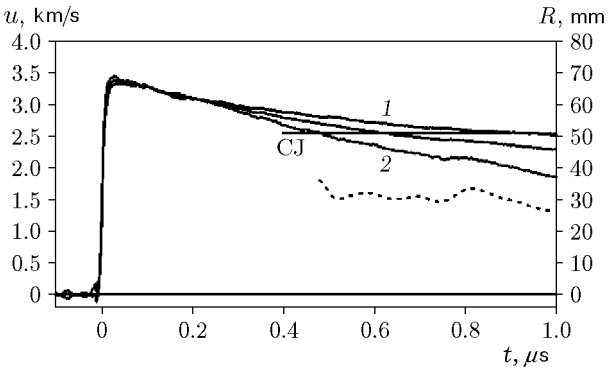

Fig. 4. Measurement results for an RDX charge of density 1.64 g/cm^3: curve *1* corresponds to the flat gauge, and curve *2* to the bent gauge.

After the retrieval of $u(t)$, the radius of curvature of the wave is also determined:

$$R = \frac{D}{u_= - u_\parallel} \int\limits_0^t u(\eta)\, d\eta. \tag{7}$$

In practice, the width of the leads s is not negligibly small and is often comparable to the length of the gauge arm L. For example, for the flat gauge described in [7], $s = 2$ mm, the total width of the gauge is 10 mm, and the cutout width (distance between leads) is 6 mm. For this ratio of dimensions, it is necessary to justify the choice of L. Furthermore, local measurements "at a given point" require reducing L to values of about 1 mm, which especially necessitates a clear definition of L. It is generally agreed that L corresponds to the midline of the gauge ($L = 8$ mm in [7]). This natural assumption is also applied in other studies [8, 9]. For the flat gauge, a theoretical justification for this choice of L is given in [10]. In the appendix below, the estimates of [10] are refined and it is shown that the same definition of the average value of L should also apply for the bent gauge.

PARTICLE VELOCITY MEASUREMENTS

In a number of experiments, various combinations of the flat and bent gauges have been tested. The most successful configuration is shown in Fig. 3.

Both gauges have a common crossbar, so that in the absence of curvature of the wave front, their readings must coincide. The output signals from the flat and bent parts were recorded by two oscilloscopes, each of which had mains-independent power supply (uninterruptible power supplies were used, which were disconnected from the power grid during the experiment). As a result, closed galvanic loops through the ground contacts that could distort measurements were eliminated.

Separate gauges turned out to be less convenient. First, their crossbars are somewhat remote from each other and therefore measure velocity at different sites. Second, the measurements revealed interference due to the capacitance between the circuits of the two measurement channels.

The gauge was cut out of aluminum foil 9 μm thick which was pre-glued on two mutually perpendicular planes of a Plexiglas block 8 mm thick. Next, the second block of the same thickness was glued, so that the leads of the bent part of the gauge passed along the gluing surface (see Fig. 3). Particular attention was paid to the gluing quality: the presence of bubbles led to the appearance of non-physical surges in records.

The measurements were performed with charges of small diameter (usually 20 mm); therefore, the gauge had a working arm length of about 1 mm. The crossbar of the gauge was located on the charge axis. The gauge was protected with an epoxy layer 50–100 μm thick. The charge was initiated by a small-size plane-wave generator. The magnetic field $B = 0.15$ T was generated by a disposable pulsed Helmholtz coil. To eliminate polarization interference, a thin grounded aluminum electrode was placed upstream and somewhat away from the gauge (at 2–3 mm). The time resolution was about 5 ns.

The result of one of the experiments is shown in Fig. 4. The pressed RDX charge was composed of separate pellets 20 mm in diameter and 10 mm high. The gauge arm was $L = 1.82$ mm, and the lead width $s = 0.57$ mm. Initially, the data of both gauges are almost the same, but over time, their readings begin to diverge, and the bent gauge gives markedly lower velocity. The profile corrected by formula (6) passes between the experimental profiles of the flat and bent gauges, closer to the former. The dashed curve shows the radius of curvature of the wave calculated by (7). Because

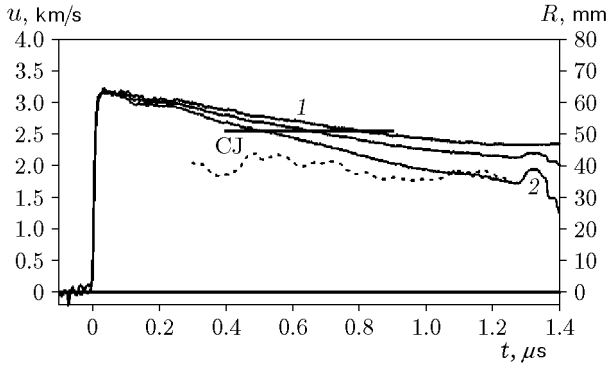

Fig. 5. Measurements results from two different experiments: curve *1* corresponds to the flat gauge with $L = 2$ mm, and curve *2* to the bent gauge with $L = 1.62$ mm.

the denominator of (7) contains the difference between the readings of the gauges, the calculation of the radius makes sense from the moment when the signals diverge significantly. Due to experimental noise, the radius somewhat fluctuates, but does not differ much from the average value of 31 mm in this experiment.

The calculated velocity in the window material (2.55 km/s) exposed to detonation products in the Chapman–Jouguet state is indicated as CJ in Fig. 4. The initial velocity is clearly above this value, demonstrating the presence of a von Neumann spike.

At some moment $t_r \simeq r^2/2RD$, the wave front reaches the part of the flat gauge located outside the charge of radius r. After that, the motion of the gauge leads changes. It is reasonable to assume that the outer part of each conductor practically does not move across the magnetic field, and the inner part continues to move in the way described above. Then, the contour in Fig. 2b still has the shape of a trapezoid, and formula (3) remains valid. For the described experiment, the time $t_r \simeq 200$ ns. As can be seen from Fig. 4, the velocity profile does not have noticeable singularities in the vicinity of 200 ns, which confirms the possibility of correcting the data using the above procedure.

If the quality of charges is sufficiently stable, it is possible to use alternately flat and bent gauges and then combine the readings of the gauges obtained in different experiments. This somewhat simplifies the preparation and performance of experiments, but doubles their number. Naturally, it is assumed that the radii of curvature will also be identical. Figure 5 shows the results of two experiments carried out with the same charges as in Fig. 4. Here the average radius of curvature was about 39 mm.

In the velocity profile of the bent gauge in Fig. 5 at $t = 1.28$ μs, the signal decline is replaced by a rise, which is caused by the motion of the leads after the wave has left the window material. This makes it possible to estimate the average wave velocity D in the correction formula (6). From the results of a series of experiments with pressed RDX, $D = 6.43$ km/s. Since the difference in the gauge signals is noticeable but not especially large (about 20%), the correction in the calculation of the true velocity also turns out to be small, and accounting for the variability of D would be unnecessary accuracy. However, the correction is needed to estimate the time to reach the CJ velocity level because the times of intersection of the profiles of $u_=$ and $u_\parallel$ with the CJ level can differ by a factor of two. The moment of intersection with the true profile $u(t)$ gives an idea of the reaction kinetics (see, e.g., [11]), and its refinement is essential.

MEASUREMENTS WITH A KNOWN CURVATURE OF THE FRONT

An advantage of the above approach is that it allows the simultaneous determination of the velocity profile and the radius of curvature of the wave front in one experiment. However, this requires information from two gauges. The radius of curvature can also be determined independently (see, e.g., [12, 13]). Then, it is enough to have a signal from only one gauge. If a flat gauge is used, from (5) we have

$$\frac{u_=}{u(t)} = 1 + \frac{1}{R}\int\limits_0^t u(\tau)\,d\tau$$

or

$$\frac{u_=}{u}\frac{d}{dt}\Big(\frac{u_=}{u}\Big) = \frac{u_=}{R}.$$

Integration of the last equality yields

$$\frac{u_=^2}{u^2} - 1 = \frac{2}{R}\int\limits_0^t u_=(\eta)\,d\eta,$$

and finally

$$u(t) = \frac{u_=(t)}{\sqrt{1 + \dfrac{2}{R}\displaystyle\int\limits_0^t u_=(\tau)\,d\tau}}. \qquad (8)$$

If the bent gauge is used, from (5) we have

$$u(t) = \frac{u_\parallel(t) + \dfrac{D}{R}\displaystyle\int\limits_0^t u(\tau)\,d\tau}{1 + \dfrac{1}{R}\displaystyle\int\limits_0^t u(\tau)\,d\tau}. \qquad (9)$$

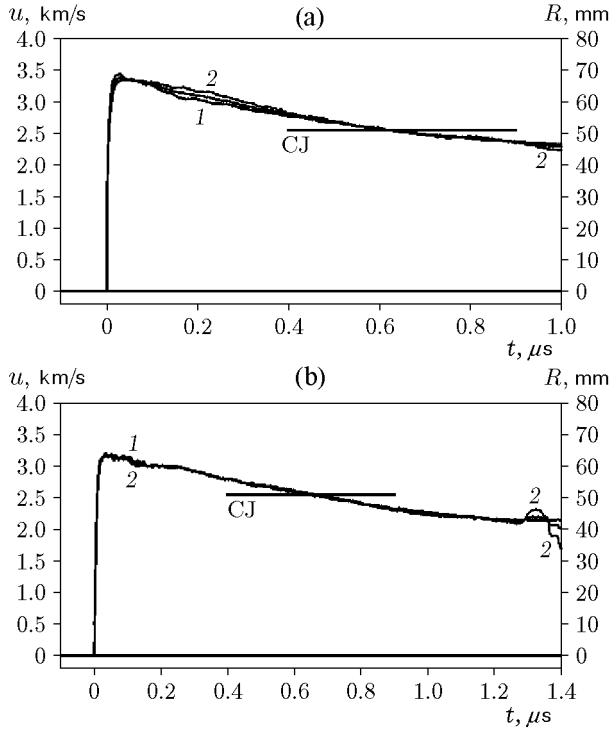

Fig. 6. Corrected profiles against the background of previously determined dependences $u(t)$ for experimental data from Fig. 4 (a) and Fig. 5 (b): curves *1* are obtained by formula (8) for the flat gauge, and curves *2* by formula (9) for the bent gauge.

Using the initial approximation $u_0(t) = u_{\parallel}(t)$, after several iterations, we obtain the refined dependence $u(t)$. Although the bent gauge is more difficult to fabricate, its advantage is that the velocity measurement is carried out locally, whereas the correction of flat gauge data implies that the radius of curvature is constant up to the surface of the charge, which is not always possible.

The application of formulas (8) and (9) to the data shown in Figs. 4 and 5 is presented in Fig. 6. The average radii of curvature for the recalculation are the same as in the previous procedure. The deviations of the corrected curves from the reference dependences $u(t)$ are small (no more than 2.5% for Fig. 6a and less than 1% for Fig. 6b). Marked differences between the curves in the latter case occur only after $t = 1.28$ μs, when the shock wave leaves Plexiglas and the recalculation procedure is no longer applicable.

The flat gauge overestimates the measured signal, and the bent one underestimates it. Of natural interest is the situation with some intermediate position of the gauge leads. Without detailing the analysis, we note here that for the flat gauge inclined at some angle α, the error vanishes at some time t_*. For the case of constant velocity u, we have

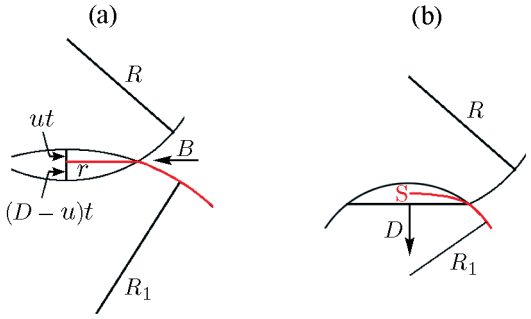

Fig. 7. Measurement geometry with the gauge placed on a convex surface: (a) formation of a flat interface; (b) formation of a flat wave front; the gauge position behind the flat front is denoted as S .

$$t_* = \frac{2R(D-u)\tan^2(\alpha)}{u^2}.$$

For example, at $R = 40$ mm, $D = 6$ km/s, $u = 2$ km/s, and $\tan(\alpha) = 0.1$, we have $t_* = 0.8$ μs. Since, at the initial time, the error also vanishes, it will be quite small (according to estimates, about 1%) within approximately 1 μs. For the variable velocity, it can be expected that the main part of the error will be eliminated. However, such a configuration with an oblique edge of the charge is obviously less convenient than those considered above.

Another method for the "instrumental" elimination of interference is to place the gauge on a curved surface whoch is convex toward the direction of wave propagation. If the wave front transforms this surface into a plane parallel to the magnetic flux vector, the deformation of the conductors will not distort the signal (Fig. 7a).

At a constant velocity u,

$$ut = \frac{r^2}{2R_1}, \qquad (D-u)t = \frac{r^2}{2R},$$

whence the radius of curvature of the surface is $R_1 = R(D/u - 1)$. Here, as in the previous version, technological difficulties arise—all the more so since at a variable velocity u, it is not possible to confine oneself to a constant curvature.

To avoid confusion, it should be noted that the above version differs from the well-known method of transforming a divergent wave front into a flat one (for which it is required to increase somewhat the curvature of the boundary). As can be seen from Fig. 7b, in such an explosive lens, the interface remains curved and cannot become parallel to the magnetic field, since the flow velocity u is always lower than the wave velocity D.

CONCLUSIONS

A modification of the electromagnetic method using a four-pin gauge was proposed that is insensitive to flow divergence. The possibility of using small-size gauges with a crossbar size of about 1 mm was substantiated. This is especially important for studies of the detonation of relatively small charges for which the detonation parameters can differ markedly from those in large charges and are relatively less studied.

Correction of readings of simpler conventional gauges is possible provided that the radius of curvature of the wave front is determined preliminarily.

The described improvements in the electromagnetic technique bring its capabilities to the level of modern interference measurements. Its "old school" image in a number of cases is not justified and largely compensated by significantly lower costs.

The author is grateful to I. A. Rubtsov for help in preparing the experiments, and to D. A. Medvedev for assistance in analyzing the response of the gauges.

APPENDIX

EFFECT OF THE FINITE WIDTH OF LEADS

Let us consider the response of the combined gauge. Fig. 8 shows it developed view. The leads of the bent gauge are placed to the right, and the crossbar and the leads of the flat part of the gauge are located to the left of the y axis.

The velocity u depends on the location (coordinate x), so that outside the charge (for the flat gauge) and ahead of the wave front (for the bent gauge) the velocity vanishes (see the graph at the top of Fig. 8). As shown in [10], the potential $\varphi(x, y)$ obeys Laplace equation $\nabla^2\varphi = 0$. At the boundaries of the gauge, the normal current density component is zero. As a result, on the horizontal (in Fig. 8) boundaries, $\dfrac{\partial\varphi}{\partial y} = Bu$.

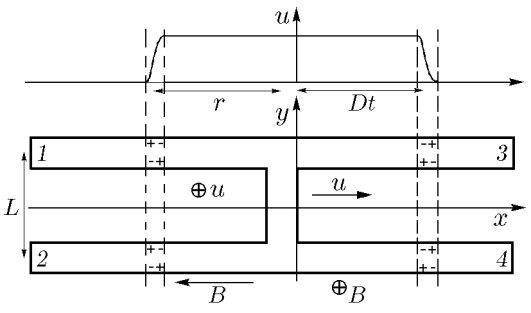

Fig. 8. Developed view of the combined gauge and schematic velocity distribution.

Suppose that at a given time the velocity of the crossbar of the gauge is equal to U. Following [10], we write the potential φ as

$$\varphi = Bu(x)y \pm \frac{BL}{2}\,(U - u(x)) + \psi, \qquad (10)$$

where L is the expected effective length of the crossbar, i.e., the distance between the midlines of the leads. In (10), the positive sign corresponds to the top leads (see *1* and *3* in Fig. 8), and the negative sign to the bottom leads (leads *2 and 4*). Within the crossbar, the second term in (10) is zero. In the fixed parts of the leads [where $u(x) = 0$], the potentials are $\pm BLU/2 + \psi$. Since BLU is the expected signal of the gauge, it remains to show that outside the moving part of the gauge, the quantity ψ can be neglected.

The equation for the correction ψ is

$$\nabla^2\psi = -B\tilde{y}\,\frac{d^2u}{dx^2}, \qquad (11)$$

where the coordinates $\tilde{y} = y \mp L/2$ are measured from the midline of the leads. In all regions of the boundary, the normal derivative ψ is zero, which justifies its introduction. The correction ψ is generated by the space charge concentrated in the regions of velocity change. The distribution of this charge is shown in Fig. 8. Of course, in practice the space charge is absent in the gauge, but for the ψ function, it occurs because ψ is not a physical potential.

We are interested in the distribution of ψ in the immovable parts of the gauge away from the charge boundary and from the wave front, where the measuring pins are attached. In these regions, for ψ we have the Laplace equation. Below, the estimates of [10] are refined and it is shown that the main part of ψ at a sufficient distance from the space charge regions has the form

$$\psi \simeq \frac{2BUs}{\pi^2}\sin\Big(\frac{\pi\tilde{y}}{s}\Big)\exp\Big(-\frac{\pi\tilde{x}}{s}\Big),$$

where $\tilde{x}$ is the distance from the boundary of motion to the considered point. Due to the exponential decay, the variable correction ψ is negligibly small when the measuring pins are removed even for a distance of the order of the width of the leads s, which is easy to do in practice. This conclusion does not depend on the form of the velocity distribution $u(x)$. Thus, the final width of the pins is not an obstacle for measurements using both the flat and bent gauges, as well as their combination.

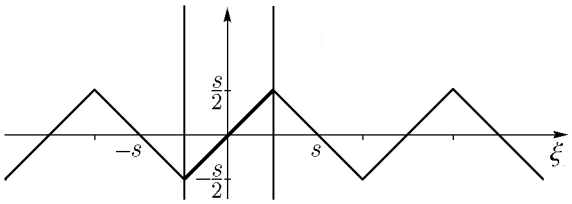

Fig. 9. Extension of the function $f(\xi) = \xi$ outside the boundary of the conductor.

The solution of Eq. (11) for the given distribution of the space charge in plane geometry

$$\rho = \varepsilon_0 B\tilde{y}\,\frac{d^2u}{dx^2}$$

has the following form [14]:

$$\psi(x,\tilde{y}) = -\frac{B}{4\pi}\int \xi \ln\left((\xi-\tilde{y})^2+(\eta-x)^2\right)\frac{d^2u}{d\eta^2}\,d\xi\,d\eta. \tag{12}$$

After a single integration over the longitudinal coordinate η, we have

$$\psi(x,\tilde{y}) = \frac{B}{2\pi}\int \xi\,\frac{\eta-x}{(\xi-\tilde{y})^2+(\eta-x)^2}\,\frac{du}{d\eta}\,d\xi\,d\eta. \tag{13}$$

In expression (13), the integration over η is extended to the space charge region (in which the velocity u changes). To satisfy the conditions on the horizontal boundaries (see Fig. 8) of the gauge, the integration over the transverse coordinate should be extended to the entire axis ξ by supplementing the charges in the physical region with image charges within the boundaries as shown in Fig. 9.

The function depicted in Fig. 9 can be represented as

$$\xi \Rightarrow f(\xi) = \frac{4s}{\pi^2}\Big(\sin\Big(\frac{\pi\xi}{s}\Big) - \frac{1}{9}\sin\Big(\frac{3\pi\xi}{s}\Big) + \frac{1}{25}\sin\Big(\frac{5\pi\xi}{s}\Big)\ldots\Big).$$

The potential ψ can be written as

$$\psi(x,\tilde{y}) = \frac{B}{2\pi}\int(\eta-x)\frac{du}{d\eta}\,d\eta\int\limits_{-\infty}^{\infty}\frac{f(\xi)\,d\xi}{(\xi-\tilde{y})^2+(\eta-x)^2}. \tag{14}$$

The integral over ξ is calculated exactly. According to [15],

$$\int\limits_{-\infty}^{\infty}\frac{\sin(k\pi\xi/s)\,d\xi}{(\xi-\tilde{y})^2+(\eta-x)^2} = \pi\frac{\sin(k\pi\tilde{y}/s)}{\sqrt{(\eta-x)^2}}\exp\left(-k\pi\sqrt{(\eta-x)^2}/s\right).$$

Consider the potential ψ within the leads *3 and 4* of the bent gauge ahead of the shock wave (for $x > Dt$). For simplicity, we assume that the gauge behind the shock wave is instantaneously accelerated to the final velocity U, so that $\dfrac{du}{d\eta} = -U\delta(\eta - Dt)$. Then,

$$\psi(\tilde{x},\tilde{y}) = \frac{2BUs}{\pi^2}\Big(\sin\Big(\frac{\pi\tilde{y}}{s}\Big)\exp\Big(-\frac{\pi\tilde{x}}{s}\Big) - \frac{1}{9}\sin\Big(\frac{3\pi\tilde{y}}{s}\Big)\exp\Big(-\frac{3\pi\tilde{x}}{s}\Big)\ldots\Big),$$

where $\tilde{x} = x - Dt$. It suffices to confine ourselves to the most slowly decaying term:

$$\psi(x,\tilde{y}) = \frac{2BUs}{\pi^2}\sin\Big(\frac{\pi\tilde{y}}{s}\Big)\exp\Big(-\frac{\pi(x-Dt)}{s}\Big).$$

Even at a distance s from the wave front, the maximum value of ψ does not exceed $2BUs\exp(-\pi)/\pi^2 = 0.0088BUs$, i.e., in the worst case, the error is a fraction of a percent of the measured value of BUL. The spread of the acceleration region of the gauge will further reduce the values of ψ ahead of the wave front.

At $x < Dt$, the potential ψ has the opposite sign and also decays with distance from the front (one should replace $x - Dt \to Dt - x$). Note that the solution (15) does not take into account the boundary conditions on the crossbar, but the rapid decay of ψ allows one to use this estimate of the error already at $Dt \simeq s$. For the flat part of the gauge, the measurement errors are all the more insignificant, since the region of velocity change is at the macroscopic distance r from the crossbar and the outer leads can always be made sufficiently long.

REFERENCES

1. Yu. N. Smirnov, "Evgeny Konstantinovich Zavoisky, a Participant of the Soviet Atomic Project," Uch. Zap. Kazan. Gos. Univ., Fiz.-Mat. Nauki **150** (3), 140–157 (2008).
2. V. M. Zaitsev, P. F. Pokhil, and K. K. Shvedov, "Electromagnetic Method for Measuring the Velocity of Explosion Products," Dokl. Akad. Nauk SSSR **132** (6), 1339–1340 (1960).
3. A. N. Dremin, S. D. Savrov, V. S. Trofimov, and K. K. Shvedov, *Detonation Waves in Condensed Media* (Nauka, Moscow, 1970) [in Russian].
4. S. G. Andreev, A. V. Babkin, F. A. Baum, et al., Physics of Explosion (Fizmatlit, Moscow, 2004), Vol. 1 [in Russian].

5. B. Hayes, "Particle-Velocity Gauge System for Nanosecond Sampling Rate of Shock and Detonation Waves," Rev. Sci. Instrum. **52** (4), 594–603 (1981); DOI: 10.1063/1.1136643.
6. J. Vorthman, G. Andrews, and J. Wackerle, "Reaction Rates from Electromagnetic Gauge Data," in *Proc. 8th Symp. (Int.) Detonation* (Albuquerque, 1985), pp. 99–110.
7. L. M. Erickson, C. B. Johnson, N. J. Parker, H. C. Vantine, et al., "The Electromagnetic Velocity Gauge: Use of Multiple Gauges, Time Response, and Flow Perturbations," in *Proc. of 7th Symp. (Int.) Detonation* (Annapolis, 1981), pp. 1062–1071.
8. P. A. Urtiew, L. M. Erickson, B. Hayes, and M. L. Parker, "Pressure and Particle Velocity Measurements in Solids Subjected to Dynamic Loading," Fiz. Goreniya Vzryva **22** (5), 113–126 (1986) [Combust., Expl., Shock Waves **22** (5), 597–614 (1986); https://doi.org/10.1007/BF00755531].
9. A. A. Vorob'ev, V. S. Trofimov, K. M. Mikhailyuk, A. N. Korolev, et al., "Investigation of Detonation Initiation in Cast Trotyl by a Dynamic Method. I. Formation of the Problem and Experimental Procedure," Fiz. Goreniya Vzryva **21** (2), 106–116 (1985) [Combust., Expl., Shock Waves **21** (2), 227–236 (1985); DOI: https://doi.org/10.1007/BF01463742].
10. A. P. Ershov, V. V. Andreev, A. O. Kashkarov, Ya. L. Luk'yanov, et al., "Detonation of Ultrafine Explosives," Fiz. Goreniya Vzryva **57** (3), 111–118 (2021); [Combust., Expl., Shock Waves **57** (3), 356–363 (2021); https://doi.org/10.1134/S0010508221030114].
11. A. P. Ershov, N. P. Satonkina, A. V. Plastinin, and A. S. Yunoshev, "Diagnostics of the Chemical Reaction Zone in Detonation of Solid Explosives," Fiz. Goreniya Vzryva **56** (6), 95–106 (2020) [Combust., Expl., Shock Waves **56** (6), 705–715 (2020); https://doi.org/10.1134/S0010508220060106].
12. E. B. Smirnov, A. N. Averin, B. G. Loboiko, et al., "Dynamics of the Detonation-Wave Front in Solid Explosives," Fiz. Goreniya Vzryva **48** (3) 69–78 (2012) [Combust., Expl., Shock Waves **48** (3), 309–318 (2012); https://doi.org/10.1134/S0010508212030082].
13. K. A. Ten, O. V. Evdokov, I. L. Zhogin, et al., "Density Distribution at the Detonation Front of Cylindrical Charges of Small Diameter," Fiz. Goreniya Vzryva **43** (2), 91–99 (2007) [Combust., Expl., Shock Waves **43** (2), 204–211 (2007); https://doi.org/10.1007/s10573-007-0028-z.
14. R. Courant, *Partial Differential Equations* (New York, 1962).
15. I. S. Gradshtein and I. M. Ryzhik, *Tables of Integrals, Sums, Series, and Products* (GIFML, Moscow, 1963) [in Russian].